Tunnelling and Underground Space Technology 161 (2025) 106538

Contents lists available at ScienceDirect

Tunnelling and Underground Space Technology incorporating Trenchless Technology Research

journal homepage: www.elsevier.com/locate/tust

Investigation of the thermal response of an energy raft foundation in Taipei ☆

Ignatius Tommy Pratama [a], Josiane Jello [b], Xin-Bai Mao [a], Kuo-Hsin Yang [a,*], Jui-Pin Tsai [c], Tugce Baser [b], Chihping Kuo [d]

[a] Department of Civil Engineering, National Taiwan University, Taipei, Taiwan
[b] Department of Civil and Environmental Engineering, University of Illinois Urbana-Champaign, Urbana, USA
[c] Department of Bioenvironmental Systems Engineering, National Taiwan University, Taipei, Taiwan
[d] Department of Civil and Construction Engineering, National Yunlin University of Science and Technology, Douliu, Taiwan

ARTICLE INFO

Keywords:
Energy raft foundation
Ground source heat pump
Heat exchange
Pipe spacing and patterns

ABSTRACT

This study investigates the thermal response of an energy raft foundation in Taipei. The energy raft foundation was installed to provide heating and cooling to a 13-story and 3-level basement residential building. The geothermal pipe comprised 40 loops connected in series and had a total heat exchange length of 6720 m. A three-dimensional numerical model was established and validated against field measurements. The thermal response of the energy raft foundation, including soil and geothermal pipe temperature distributions, was investigated. A series of parametric studies was conducted to evaluate the effects of the geothermal pipe spacing and pattern on the heat exchange efficiency. The results from numerical simulations indicated that the pipe outlet fluid temperature varied during the daily operation cycle. The maximum and minimum temperature differences between the inlet and outlet fluid temperatures were 7 and 4 °C, occurring at the beginning and the end of daily operations, respectively. The horizontal range of influence of the geothermal pipe on the soil temperature was small at approximately 1.6 times the width of the pipe loop, suggesting that the geothermal pipe would have little effect on the soil temperature in an adjacent building's foundation. The pipe spacing and pattern strongly influenced the heat exchange efficiency. For the snake and swirl patterns with separate high- and low-temperature pipes, the pipe outlet fluid temperature was lowest for a pipe spacing of $S = 0.1$ m. For the meander and loop patterns, the influence of adjacent pipes resulted in a higher outlet fluid temperature at $S = 0.1$ m than at $S = 1.0$ m. On the basis of this study's findings, the optimal pipe configuration is discussed.

1. Introduction

Shallow geothermal systems leverage the heat stored in the shallow subsurface to provide efficient and sustainable solutions to heating, cooling, and hot water needs while reducing dependency on fossil fuels (Lund and Toth, 2021; Reiter et al., 2023; Jello and Baser, 2023). An energy foundation is a type of shallow geothermal system that provides structural support for a superstructure and acts as a heat exchanger (Laloui and Loria, 2019; Cunha and Bourne-Webb, 2022). Energy foundations can be integrated with piles (Reiter et al., 2020; Ghasemi-Fare and Basu, 2013), raft-pile foundations (Fang et al., 2020), walls (Bourne-Webb et al., 2016), and tunnels (Barla et al., 2019). These systems not only offer environmental benefits but can also lead to substantial cost savings; their energy costs can be up to 16 times lower than those of natural gas or electrical systems (Khan and Wang, 2014).

Many researchers have extensively studied energy piles over the past several decades (Moradshahi et al., 2022; Faizal et al., 2019; Caulk et al., 2016; Khosravi et al., 2016). Sani et al. (2019) presented an extensive review of the performance of energy pile foundations and concluded that this performance is affected by many factors, including thermal conductivity, groundwater flow, soil moisture content, the number and configuration of energy loops, and pile length and diameter. Faizal et al.

☆ This article is part of a special issue entitled: 'Sustainable Underground' published in Tunnelling and Underground Space Technology incorporating Trenchless Technology Research.

* Corresponding author at: Department of Civil Engineering, National Taiwan University (NTU), 1, Sec. 4, Roosevelt Rd., Taipei 10617, Taiwan.
E-mail addresses: tommyignatius@unpar.ac.id (I.T. Pratama), jjello2@illinois.edu (J. Jello), r11521115@ntu.edu.tw (X.-B. Mao), khyang@ntu.edu.tw (K.-H. Yang), jptsai@ntu.edu.tw (J.-P. Tsai), tbaser@illinois.edu (T. Baser), cpkuo@yuntech.edu.tw (C. Kuo).

https://doi.org/10.1016/j.tust.2025.106538
Received 2 May 2024; Received in revised form 4 February 2025; Accepted 28 February 2025
Available online 5 March 2025

(2022) performed a field test on a bored energy pile with installed sensors to measure the radial temperature distribution from the heat exchanger pipes to the soil. The pile and thermal resistances were affected by the pile dimensions, number of pipes, concrete cover, and soil types. Additionally, Brandl (2006) found that the concrete's composition, including the cement's fineness and additives, influences the heat exchange rate. The heating and cooling cycles also affect the amount of energy exchanged. Specifically, in intermittent operation (8 h of heating per day), 40.9 % more energy was found to be extracted per meter than was in a continuous 24-h heating mode (Singh et al., 2015). In a similar study, monotonic and cyclic heating and cooling were investigated. The findings showed that cyclic heating and cooling led to smaller ground temperature changes due to thermal recovery between cycles. This suggests that cyclic heating and cooling can improve geothermal energy utilization and lower the impact on the ground in the long-term operation (Faizal et al., 2018; 2020; 2021; Casagrande et al., 2022).

Changes in the water content of unsaturated soil affect its thermal conductivity, in turn affecting the thermal performance of a pile and the transfer of heat between the pile and soil (Coccia and McCartney, 2016; Baser et al., 2018, McCartney et al., 2014). An investigation of the performance of energy group piles revealed that their heat injection and extraction rates were 5 % and 20 % lower, respectively than those for a single pile (You et al., 2016). Behbehani and McCartney (2022) investigated the response of an energy group pile in unsaturated soil at high temperatures (~90 °C) by using a validated thermo-hydraulic numerical model. The results suggested that the water table depth and hydraulic properties controlled the heat transfer rate and amount of total heat stored. Other work has focused on the behavior of energy pile-raft foundation systems (Fang et al., 2020; Amirdehi and Shooshpasha, 2022; Mehrizi et al., 2016); the results have revealed that the parameters affecting the system response include the raft's stiffness, the displacement ratio between the raft and single piles, and the piles' slenderness coefficient.

Energy walls have also been studied in recent years, focusing on their thermo-hydraulic behavior. Di Donna et al. (2021) performed numerical simulations of energy walls by using a coupled thermo-hydraulic model based on the finite element method. They developed design charts that can be used to estimate the energy capacity of energy walls. Furthermore, they reported that the factors that most strongly affect the heat exchange rate are the groundwater flow velocity and the difference between the undisturbed soil and fluid circulation temperatures. In a case study conducted by Angelotti and Sterpi (2020) in Italy in 2016, on-site monitoring data and numerical simulations were combined to understand the processes of the transfer of heat between the pipes and surrounding boundaries. The soil acted as a heat source and sink during heating and cooling cycles, respectively, and the basement absorbed heat from the fluid during heating and transferred heat during cooling.

Energy tunnels have also been investigated in several studies. Insana and Barla (2020) developed a thermo-hydraulic numerical model and calibrated it by using data collected from a real-scale energy tunnel prototype tested in the Turin Metro Line 1 South Extension. The results indicated that groundwater flow improves heat transfer and that the inlet fluid temperature significantly influences design considerations.

A wide body of research has focused on various energy foundation systems. However, energy raft foundations remain in their infancy, and only a few studies have performed behavior analyses for these foundations (Moon and Choi, 2015; Lee et al., 2018; Lee et al., 2021). In a series of field tests, Lee et al. (2018) investigated the influence of the pipe material [i.e., high-density polyethylene (HDPE) and stainless steel, each with a unique pipe pattern] on the thermal performance of energy slabs. The results indicated that higher thermal conductivity of the geothermal pipe resulted in higher performance of the energy slabs. Lee et al. (2021) conducted a series of numerical parametric studies on the factors affecting the performance of energy slabs. The results revealed that the soil's thermal conductivity and the flow rate of the geothermal pipe fluid were the influential factors, while the thermal conductivity of the concrete slabs did not significantly influence the performance of the energy slabs. However, the previous study did not fully investigate the thermo-hydraulic response during heating and cooling cycles for different pipe configurations.

This paper presents a unique case study of an energy raft foundation in New Taipei City, Taiwan. The geothermal pipe configuration comprised 40 connected loops in series with a combined length of 6720 m. The geothermal pipes were equipped with temperature sensors to measure the inlet and outlet fluid temperatures during operation. Data from the field installation were used to calibrate a three-dimensional coupled thermo-hydraulic numerical model. The model was then used to perform a parametric study to investigate the influences of geothermal pipe spacing and pattern on heat exchange efficiency. Finally, the calibrated numerical model results were analyzed to advance the understanding of the behavior and performance of energy raft foundations.

2. Case study of energy raft foundation

2.1. Description of the case study

During summer in Taiwan, demand for air conditioning is high, straining the power supply. Furthermore, the heat generated by air conditioning systems contributes to rising ambient temperature, exacerbating the urban heat island effect in Taipei. Energy foundations have emerged as promising renewable energy technologies to tackle these challenges. In this study, a unique energy raft foundation for a 13-story residential building with a 3-level basement in Taipei, Taiwan, was constructed to reduce the electricity consumed by air conditioning units in the residential building. Fig. 1 shows the details of the construction of the energy foundation.

The energy raft foundation investigated in this case study comprised a raft foundation, ground source heat pumps (GSHPs), and ground heat exchangers (GHEs). The raft foundation had dimensions of 54.3 m × 23.5 m and was constructed 11.8 m below ground level. In the excavation of the foundation, soldier piles and lagging walls were used as the earth-retaining structure. Two GSHPs were installed in the basement to meet the minimum cooling load demand of approximately 240 kW for the building. The GSHPs operated daily for 10 h during the daytime and were turned off for the rest of the day.

The GHEs used in the case were geothermal pipes made of HDPE with a diameter of 32 mm. HDPE pipe was selected instead of metal pipes because of its higher workability, flexibility, durability, and high-pressure resistance. In addition, HDPE has higher thermal conductivity than other typical polymer materials used for pipes (Mendrinos et al., 2017). The geothermal pipes were installed beneath the raft foundation approximately at the interface between the reinforced concrete slab and soil, and the pipes covered an area of approximately 49.3 m × 19.8 m. The geothermal pipes were arranged as 40 loops connected in series with a total length of 6720 m. The spacing between the pipes was approximately 0.1 to 0.2 m. In the configuration, the fluid in the first half of the pipe loop flowed counterclockwise toward the center of the pipe pattern. In the second half of the loop, the fluid flowed in the clockwise direction toward the pipe outlet. In this pipe configuration, each loop had a different length; the outermost loop was the longest, and the innermost loop was the shortest.

The process for constructing the energy raft foundation is outlined as follows. After the excavation of the foundation had reached the bottom of the raft foundation, the geothermal pipes were installed by layering them on top of wire mesh mattresses and then securing them in position by tying them to the wire mesh (Fig. 1a and 1b). To minimize the risk of water leakage, a series of leak tests were performed on each loop of the geothermal pipes. During the leak test, the water inside the pipe was gradually pressurized to 800 kPa, and the pipes were then carefully inspected to ensure that no leakage occurred (Fig. 1c). Once all the

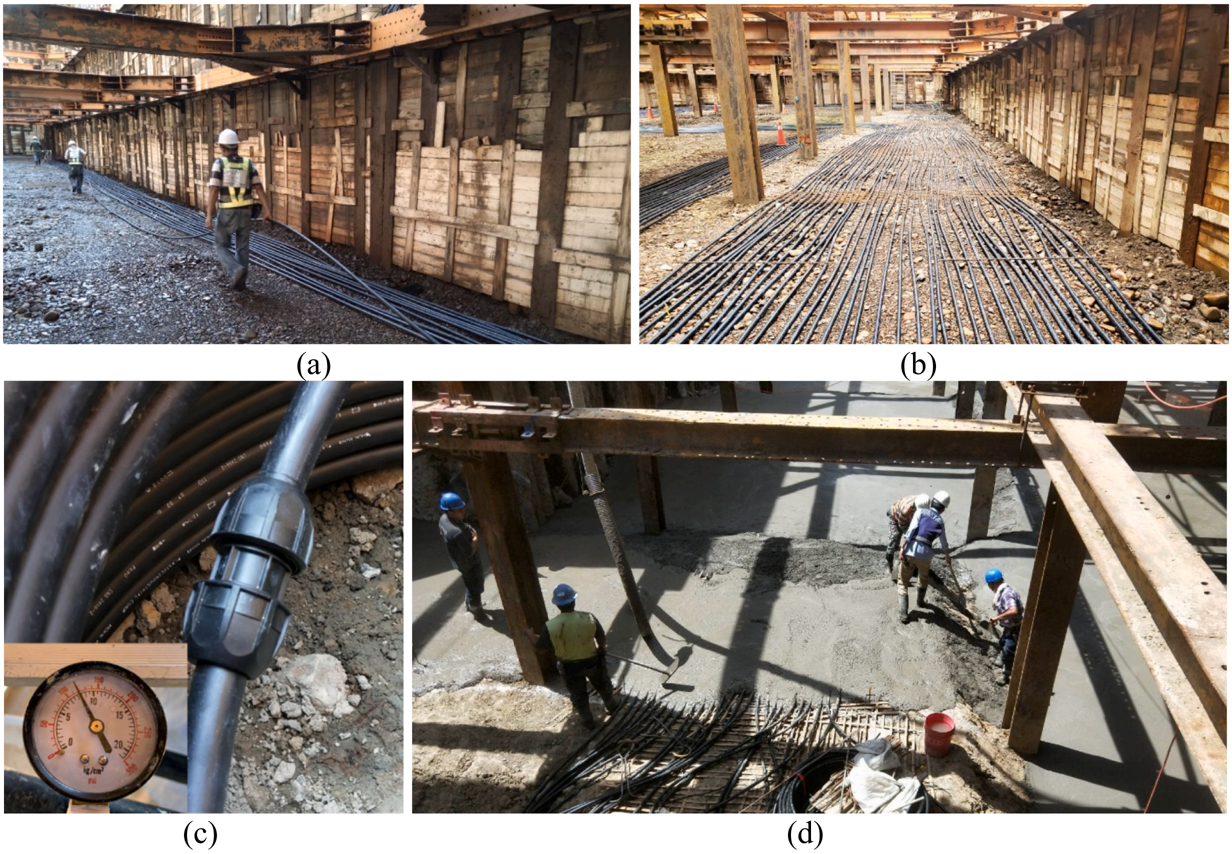

Fig. 1. Construction of energy raft foundation in Taipei: (a) layering geothermal pipe; (b) geothermal pipe configuration; (c) leak test by pressurizing up to 800 kPa; (d) spreading shotcrete to protect the geothermal pipe.

geothermal pipes had been placed, a layer of shotcrete was spread on top of them to protect them from possible damage during construction of the raft foundation above (Fig. 1d).

2.2. Subsurface soil conditions

The energy raft foundation was constructed on top of young alluvial deposits from the Holocene period, which are commonly distributed along riverbanks in the Taipei Basin. According to the borehole data, the subsurface soil layers at the construction site were five alternating layers of sand and gravel. The first layer was a backfill layer (SF), which was 0–3.4 m below ground level. The backfill layer primarily comprised a mixture of natural soil, stone, and crushed concrete from previous construction activities. The second layer was a loose silty sand (SM) layer located at a depth of 3.4–4.6 m. The average standard penetration test (SPT) value of this layer was found to be SPT-N = 8. The third layer was a dense gravel layer (G) located at a depth of 4.6–17.4 m and with an average SPT-N value of ≥50. The raft foundation was situated on this gravel layer at a depth of 11.8 m because of the substantial bearing capacity of the firm gravel layer. The fourth layer was a medium silty sand layer (SM) at a depth of 17.4 m–21.7 m and with an average SPT-N value of 16. The fifth layer was a dense gravel layer (G) with an average SPT-N value of ≥50. Table 1 lists the soil profile and properties obtained from the site investigation report. Table 2 lists the input soil thermal and hydraulic properties. The values of the soil's thermal and hydraulic properties were estimated on the basis of the values reported in the literature for similar soils (Alnefaie and Abu-Hamdeh, 2020; Cao et al., 2018; Fang and Chien, 2004; Santa et al., 2017).

The groundwater level was monitored using observation wells and piezometers. The observation wells extended to 35 m from the surface, and the piezometer measurements were collected at a depth of 25 m. Groundwater level measurements were taken weekly at each location and continued for several months after installation. On the basis of the field measurements, the groundwater was detected at depths of approximately 12.6 and 13.7 m.

Fig. 2 shows the average soil temperature profile in Taipei. According to the study by Liu (1974), the average soil temperature at ground level was 31 °C in summer and 15 °C in winter. These soil temperature

Table 1
Soil profile and properties.

Depth (m)	Layer ID	USCS	SPT-N	Index properties			Shear strength properties	
				Water content ω (%)	Unit weight γ_t (kN/m^3)	Void ratio e	Cohesion c (kN/m^2)	Friction angle ϕ (°)
0.0–3.4	I	SF	–	–	20	–	0.0	30.0
3.4–4.6	II	SM	8	16.7	20	0.56	0.0	29.1
4.6–17.4	III	G	>50	–	22	–	10	35.0
17.4–21.7	IV	SM	16	17.0	20	0.51	0.0	31.6
21.7–25.0	V	G	>50	–	23	–	10	38.0

Table 2
Input thermal and hydraulic properties.

Depth (m)	Layer ID	Material	Thermal conductivity λ (W/m·K)	Heat capacity C_p (J/kg·K)	Hydraulic conductivity k (m/s)
0.0–3.4	I	Backfill	1	800–1600	10^{-4}
3.4–4.6	II	Silty sand	0.6	800–1600	10^{-5}
4.6–17.4	III	Gravel	0.6 (above GWT) 2.4 (below GWT)	1200–1600	10^{-3}
17.4–21.7	IV	Silty sand	1.4	800–1600	10^{-5}
21.7–25.0	V	Gravel	2.4	1200–1600	10^{-3}
9.8–11.8	–	Concrete	2.5	850	-
0.00–11.8	–	Air	0.03	1005	-

values align closely with the measured data conducted by the Taiwan Central Weather Administration in 2023. Generally, soil temperature decreases with depth in summer but increases with depth in winter. The soil temperature is constant at 24 °C at depths greater than 3 m, regardless of the season.

3. Numerical analyses

3.1. Mathematical formulation

To characterize the coupled thermo-hydraulic processes during the operation on an energy raft foundation installed in a soil profile, a system of equations describing coupled physical processes of heat transfer in pipes, heat transfer in soil, and subsurface flow is required. Based on the conservation of energy in pipe flow, the governing equation for heat transfer in pipes is expressed in Eq. (1) as follows (Bejan, 2013; COMSOL Multiphysics, 2023a):

$$\rho_f A_f C_{p,f} \frac{\partial T_f}{\partial t} + \rho_f A_f C_{p,f} u e_t \cdot \nabla T_f = A_f \lambda_f \nabla \cdot (\nabla T_f) + f_D \frac{\rho_f A_f}{2 d_h} |u| u^2 + Q_{pw} \tag{1}$$

where ρ_f is the fluid density (kg/m^3), A_f is the cross-section area of flow (m^2), $C_{p,f}$ is the fluid-specific heat (J/kg·K), u is the circulating fluid flow velocity (m/s), e_t is a unit tangent vector to the pipe axis, T_f is the fluid temperature (K), t is the time, λ_f is the fluid thermal conductivity (W/m·K), d_h is the hydraulic diameter of the pipe (m) that can be estimated by $d_h = 4A_f/P$ with P as the wetted perimeter (m), f_D is the Darcy friction factor (dimensionless) – a function of Reynold number (Re), surface roughness (e) (in m), and d_h, and Q_{pw} describes the external heat exchange through the pipe wall (W/m), which is described in Eq. (2) as follows:

$$Q_{pw} = hZ(T_{s,ext} - T_f) \tag{2}$$

where h is the effective heat transfer coefficient (W/m^2·K) related to the thermal conductivity of the pipe λ_w (W/m·K) and pipe wall thickness b (m), Z is the perimeter of the pipe wall (m), and $T_{s,ext}$ is the soil temperature external to the pipe wall (K). In this study, $T_{s,ext}$ was higher than T_f because the heat injection process through the geothermal pipe was simulated. Eq. (1) describes the heat transfer in a pipe flow system using a 1D model to define the pipe flow profile and temperature profiles on curve segments or lines. The left-hand side terms (LHS) terms of Eq. (1) represent the heat accumulation in fluid (Q_{ha}) and convective heat transfer in the moving fluid (Q_{cv}), while the right-hand side (RHS) terms of Eq. (1) capture heat conduction within the fluid (Q_{cd}), thermal energy induced by fluid friction (Q_{ff}), and heat exchange at the pipe wall (Q_{pw}) which is estimated using Eq. (2). These terms describe the combined effects of heat transport mechanisms in the fluid (convection and conduction) and the heat transfer between the fluid, the pipe wall, and the external environment or soil in this study. The unit of each term in Eq. (1) (i.e., W/m) represents heat transfer rate per unit pipe length, quantifying heat flow at any point along the pipe. Fig. 3 illustrates the heat transfer mechanism in a pipe and the components considered in Eqs. (1) and (2).

Based on the energy balance in the porous media (COMSOL Multiphysics, 2023b), the general governing equation for heat transfer in a porous matrix is expressed using Eq. (3) as follows:

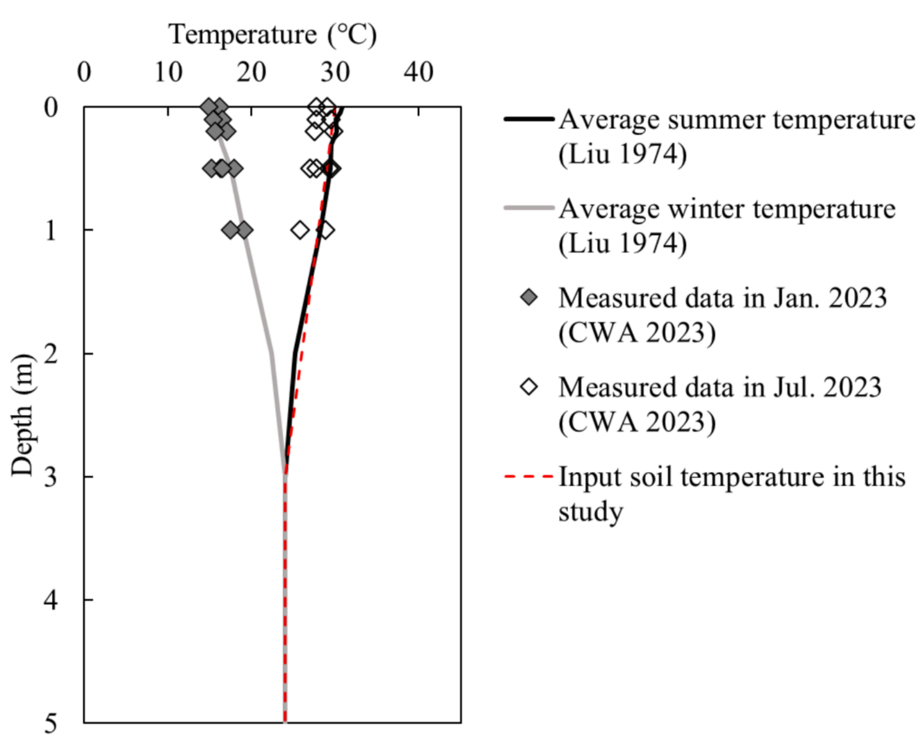

Fig. 2. Soil temperature profile in Taipei.

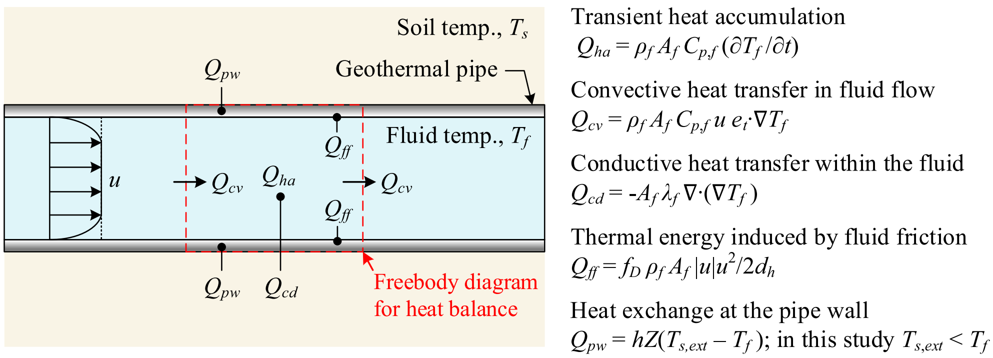

Fig. 3. Schematic diagram of the mechanism of heat transfer in pipe.

$$\rho_s C_{p,s} \frac{\partial T}{\partial t} + \rho_f C_{p,f} u \cdot \nabla T + \nabla \cdot (-\lambda_s \nabla T) = Q \tag{3}$$

where ρ_s is the density of soil (kg/m^3), $C_{p,s}$ is the specific heat of soil (J/kg·K), λ_s is the thermal conductivity of soil (W/m·K), u is the Darcy velocity of flow through the media (m/s), T is the temperature of both fluid and solid phases (K), and Q is the internal volumetric heat generation (W/m^3). The unit of each term in Eq. (3) (i.e., W/m^3) represents the heat transfer rate per unit volume of a porous material. Notably, Eq. (3) was applied to the soil and raft foundation with distinct material parameters (see Table 2), and the fluid velocity u equals zero.

Subsurface fluid flow is governed by Darcy law (COMSOL Multiphysics, 2023c) and is expressed using Eqs. (4) and (5) as follows:

$$u = \frac{-k}{\rho_f g} (\nabla p + \rho_f g) \tag{4}$$

$$\nabla \cdot (\rho_f u) = 0 \tag{5}$$

where k is the hydraulic conductivity of the soil (m/s), g is the gravitational constant (m/s^2), and p is the pore pressure (Pa).

3.2. Numerical model and settings

A three-dimensional finite element method was developed in COMSOL Multiphysics v6.2 to simulate the thermal response of the energy raft foundation during heating (heat injection) in summer. Fig. 4 presents the model's geometry, including the mesh configuration, geothermal pipe layout, and boundary conditions. First, the soil layers were modeled at depths based on those in the soil investigation report (Table 1) and as solid blocks by using the Block interface in COMSOL. The raft foundation with dimensions of 54.3 m × 23.5 m × 2 m was then modeled in a soil domain of dimensions 70 m × 40 m × 25 m (Fig. 4a). The dimensions of the soil domain were determined through boundary influence analyses to ensure that the model boundaries did not influence the thermal response of the energy raft foundation. The boundaries in the x- and y-directions were set at distances of 7.85 and 8.25 m, respectively, from the earth-retaining structure, and the bottom boundary was placed 13.2 m below the raft foundation. These distances were deemed sufficient for heat transfer without the boundaries having an influence. The range of the geothermal pipe's influence on the soil temperature is discussed in Section 4.2.

The raft foundation comprised the soldier pile and lagging walls, marked as the earth-retaining structure in Fig. 4a, and the base slab. The model of the soldier pile and lagging walls was simplified to a vertical slab with no depth below the base slab because detailed data regarding the wall configuration were unavailable. The thickness of the earth-retaining structure was $t_w = 0.5$ m, and the thickness of the base slab was $t_s = 2$ m. The basement above the raft foundation was modeled as a solid block with the dimensions 53.3 m × 22.5 m × 9.8 m.

The geothermal pipe was modeled as a sequence of connected line segments by using the Polygon interface in the COMSOL program. The geothermal pipe was located below the raft foundation at 12 m below ground level, which was consistent with the construction in the field. As shown in Fig. 4b, a loop pattern was adopted for the geothermal pipe pattern; the fluid flowed counterclockwise in the first half of the pipe loop and clockwise toward the pipe outlet in the second half. The pipe was installed as 40 loops connected in series with a pipe spacing of $S =$ 0.1 m and a total length of 6720 m. The inner diameter of the pipe was 2.74 cm, and the pipe thickness was $b = 2.3$ mm. The thermal conductivity of the pipe was set to $\lambda_w = 0.4$ W/m·K, which is a typical value for HDPE. A tetrahedral mesh was generated for the entire model with an average element size of 1.7 m. The geothermal pipe and raft foundation were situated in layer III, the gravel layer (Table 1); thus, the mesh size in this layer was finer at an average element size of 0.6 m because heat exchange mainly occurred in this soil layer. The smaller mesh size in this layer was also necessary because of the small pipe spacing ($S = 0.1$ m) and the distance between the pipe and the raft (0.2 m). Mesh refinement was not performed for the other soil layers because, given their thermal properties (Table 2) and distance from the geothermal pipe, the influences of the geothermal pipe on these layers would be weak. The influence of the geothermal pipe is further discussed in Section 4.2. The aforementioned mesh configuration resulted in 1,408,660 elements.

The Heat Transfer in Porous Media interface was used to simulate heat transfer in the soil, raft foundation, and basement. The field measurements from the case study were obtained in summer; thus, the soil temperature profile depicted by the red dashed line in Fig. 2 was used to define the initial soil temperature $T_{initial}$. The initial soil temperature decreased with depth and was 24 °C for all depths greater than 3 m. The heat transfer within the geothermal pipes was simulated using the Heat Transfer in Pipes interface. A constant inlet fluid temperature of $T_{in} =$ 39 °C (i.e., heat injection) was maintained throughout the 4-week operation. The inlet fluid temperature was determined based on the measured inlet fluid temperature in the case study. Fig. 5 shows the measured and input pipe inlet fluid temperatures. Furthermore, the external pipe temperature in the model was coupled to the soil temperature, meaning that heat could be transferred between the pipe and the soil.

The GSHP was simulated as operating for 10 h/day over 28 days. During operation, the inlet fluid inside the pipe circulated with a discharge of 50 L/min (a fluid velocity of 1.413 m/s); no fluid flow was included in the model when the pump was not operating. The pumping power required to circulate fluid in geothermal pipes can influence the performance of energy raft foundations (Lee et al., 2021; ten Bosch et al., 2024). The design of the geothermal pipe pattern, including its length and spacing, can also cause pressure losses; thus, more pumping power may be required when the pattern is complex. However, the influence of pumping power on the performance of the energy raft foundation was beyond the scope of this study. Thus, the GSHP system was assumed to have sufficient pumping power to circulate the fluid effectively.

Fig. 4c presents the initial and boundary conditions. The constant-

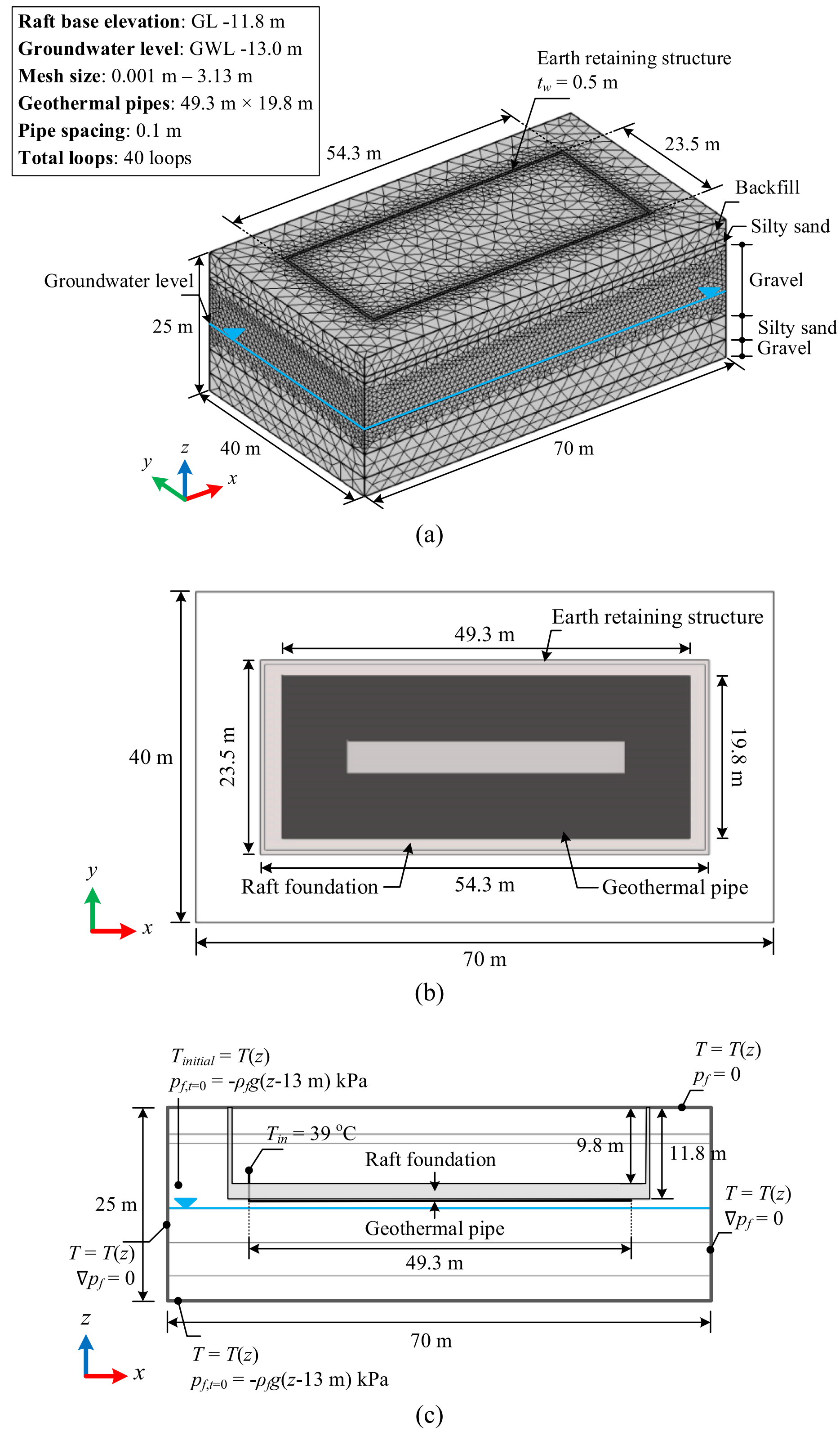

Fig. 4. Numerical model: (a) model and mesh configurations; (b) geothermal pipe configuration; and (c) boundary conditions.

temperature boundary condition $T = T(z)$ was applied to the exterior boundaries of the soil domain; that is, the temperature at these boundaries was assumed to remain stable over time, and the operation of the energy raft foundation system did not influence the thermal state of these boundaries. A similar approach has been applied in related studies (e.g., Insana and Barla, 2020; Di Donna et al., 2021; Zhong et al., 2023). No thermal boundary was applied to the pipe, raft foundation, or adjacent soil to allow heat to transfer freely. The groundwater level at 13 m below ground level was modeled using the Darcy's Law interface in COMSOL. Constant hydrostatic pressure was applied throughout the soil domain to a depth of 13 m to simulate the actual groundwater conditions. The exterior boundaries of the soil domain were set to be

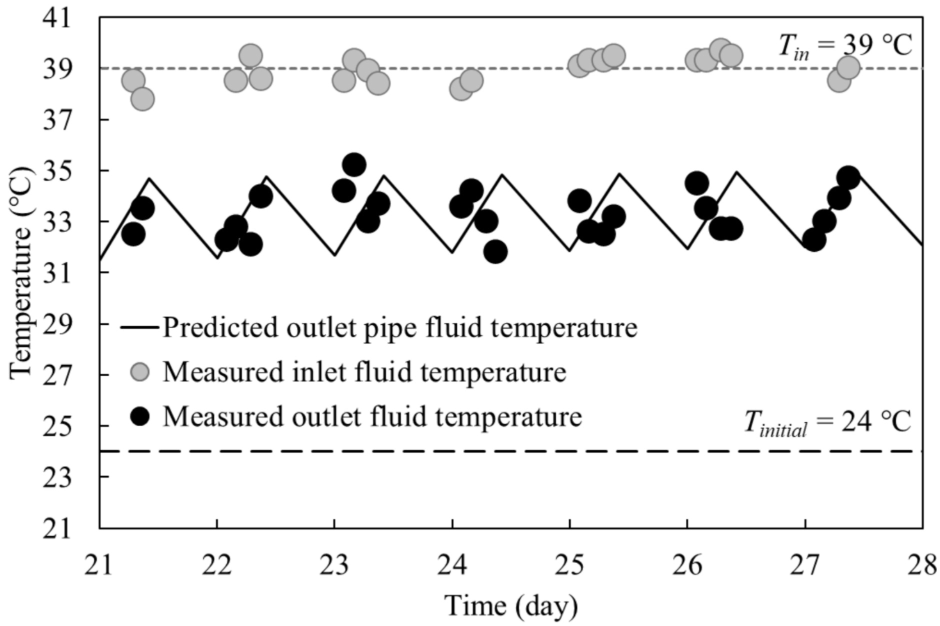

Fig. 5. Comparison of measured and predicted geothermal pipe outlet fluid temperatures.

impervious; no flow could cross the boundaries. At the bottom of the model, a pressure boundary was applied to model the pore water pressure corresponding to the groundwater table at 13 m below ground level.

4. Results and discussion

4.1. Numerical model validation

The numerical model developed in this study was first validated against the measured data collected in the field. The outlet fluid temperatures from the numerical simulations were compared with the measured fluid temperatures. The comparison focused on days 21 to 28 because the outlet fluid temperature reached a steady state after 3 weeks of operation, at which point the soil temperature increased by less than 3 %. In the simulations, the GSHP system was operated for 10 h/day for 28 days. Longer and higher heat injections would likely produce different results (Zhong et al., 2023; ten Bosch et al., 2024) and lead to a different duration to reach the steady state. Further investigation on the long-term thermal response of energy raft foundations in various soil conditions should be conducted in future research.

Fig. 5 presents the measured and simulated outlet fluid temperatures. The results show that upon the heat injection, the predicted pipe outlet fluid temperature increased and reached its peak after 10 h of operation. The pipe outlet fluid temperature decreased when the heat pump was not operating, achieving a peak-to-valley temperature difference at a steady state of 3 °C. The maximum and minimum temperature differences between the inlet and outlet fluid temperatures were 7 and 4 °C at the beginning and end of the daily operation, respectively. As shown in Fig. 5, the measured data exhibited slight fluctuations because of changes in the inlet fluid temperature; however, the simulated outlet fluid temperature values were generally in close agreement with the measured values. This correspondence suggested that the numerical model effectively captured the actual thermal behavior of the geothermal system and could be further used to investigate the thermal and hydraulic behavior of the system of interest.

4.2. Thermal response of the energy raft foundation

Once it had been validated, the numerical model was used to evaluate the thermal response of the energy raft foundation. Fig. 6 presents the geothermal pipe temperature distribution contour at day 28. Upon initiation of heating, a high-temperature influence zone was found near the pipe inlet that reached a temperature of 38.5 °C. The temperature then gradually decreased as the fluid inside the geothermal pipe flowed toward the center of the loop, reaching a temperature of 29 °C. This indicated the transfer of heat from the pipe to the surrounding soil. As the fluid continued flowing in the outlet direction (clockwise) toward the pipe outlet, the pipe temperature rose, reaching a temperature of 32.2 °C due to the influence of the adjacent pipes (S = 0.1 m). The influence of the pipe spacing is further discussed in Section 5.1.

Fig. 7 presents the soil temperature over time in longitudinal and transverse cross sections. The soil temperature data were measured near the depth of the geothermal pipe. Fig. 8 shows the change in soil temperature profile at the center of the pipe loop over time. Fig. 9 presents an overview of the soil temperature distribution contours in the horizontal and vertical cross sections. The results revealed that the soil temperature increased over time and that the maximum soil

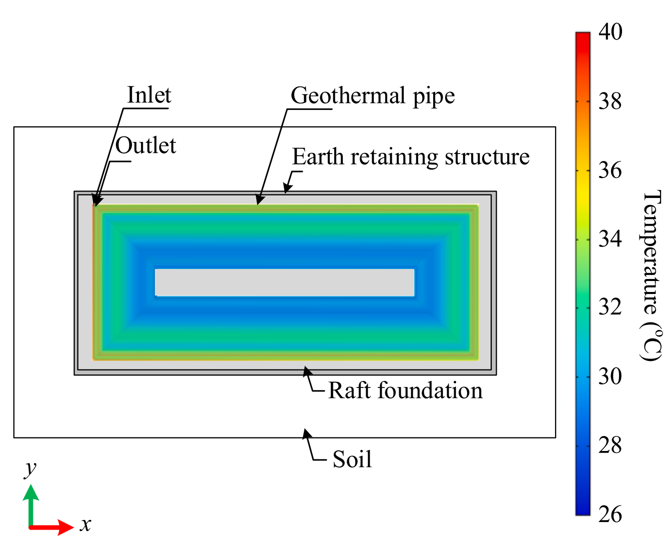

Fig. 6. Geothermal pipe temperature distribution contour.

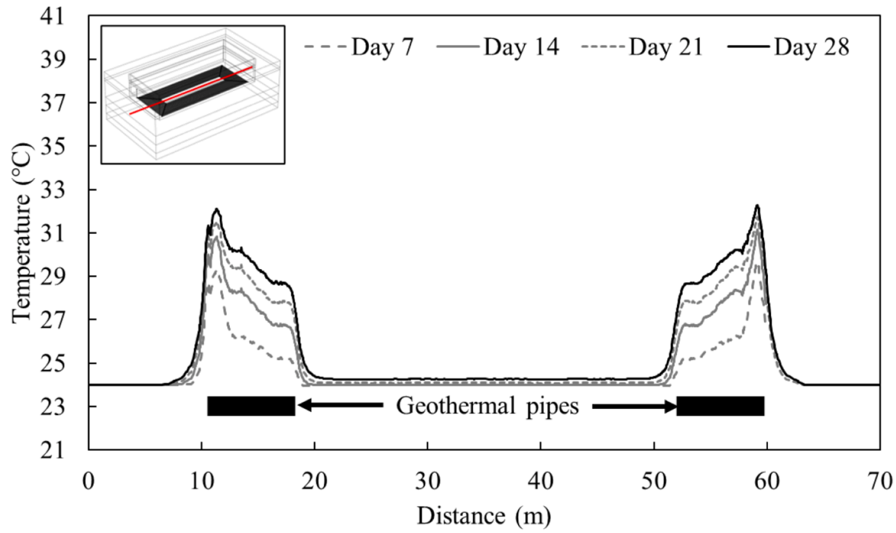

(a)

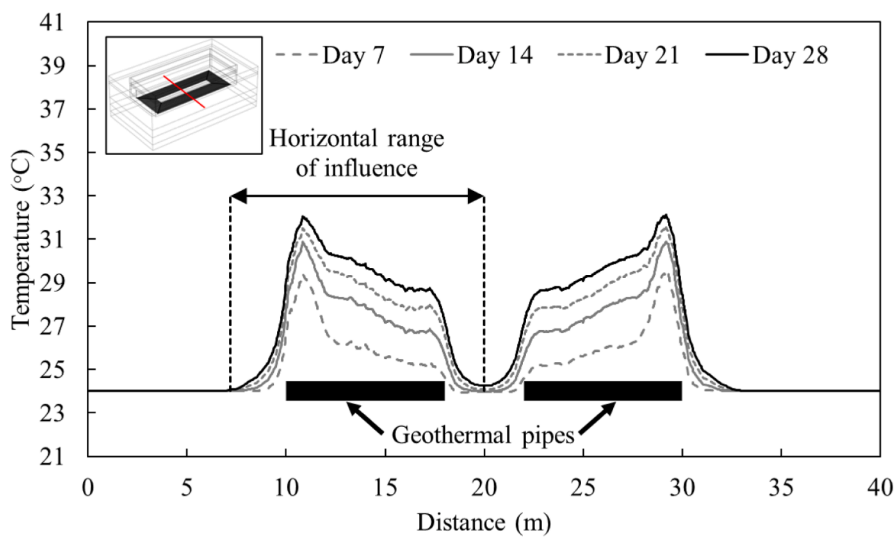

(b)

Fig. 7. Soil temperature distributions along (a) the longitudinal cross-section and (b) the transverse cross-section.

temperature reached a steady state in which the soil temperature rose less than 3 % (Fig. 7a). The temperature of the soil at the center of the pipe loop was less influenced by the geothermal pipe's temperature increase than that of the soil near the geothermal pipe because the low thermal conductivity of dry soil hindered heat propagation (Fig. 7b). The horizontal range of influence was found to be relatively small, being approximately 1.6 times the width of the geothermal pipe loop. These results suggest that the geothermal pipe had little influence on the temperature of the soil near the adjacent building's foundation (Figs. 7 and 9).

The soil temperature profiles at the center of the geothermal pipe pattern also indicated an increase in the temperature with time, reaching a peak of 24.5 °C on day 28 (Fig. 8). The vertical influence of the geothermal pipe on its surroundings had a range of approximately 3.5 m above and below the pipe depth. The highest soil temperature occurred within the concrete raft foundation due to its higher thermal conductivity than that of the surrounding soil and air. The soil temperature distribution contour in Fig. 9b also shows a nonuniform temperature increase within the raft foundation and concentrations of high temperature near the edge of the raft foundation. These nonuniformities in the temperature increase could induce changes in the mechanical behaviors of the raft foundation, affecting the stability and serviceability of the structures. Thus, a further investigation into the mechanical behavior of the energy foundation, such as the thermal-induced stress in the concrete slab and the reaction force from the thermal expansion acting on the soil, should be conducted in future research.

Fig. 10 shows the variations in the outlet fluid and soil temperatures during heat injection. The outlet fluid and soil temperatures increased over time and reached a steady state after 3 weeks of operation. The outlet fluid temperature increased during heating and decreased when the pump was not operating; the average temperature difference between the maximum and minimum temperatures in a steady state was 3 °C. Similarly, the soil temperature increased upon heat injection and decreased when the pump was not operating, with the temperature difference between the maximum and minimum outlet fluid temperatures in a steady state being 0.5 °C. The results indicated that the magnitude of the soil temperature variation depended on the heat capacity of the soil.

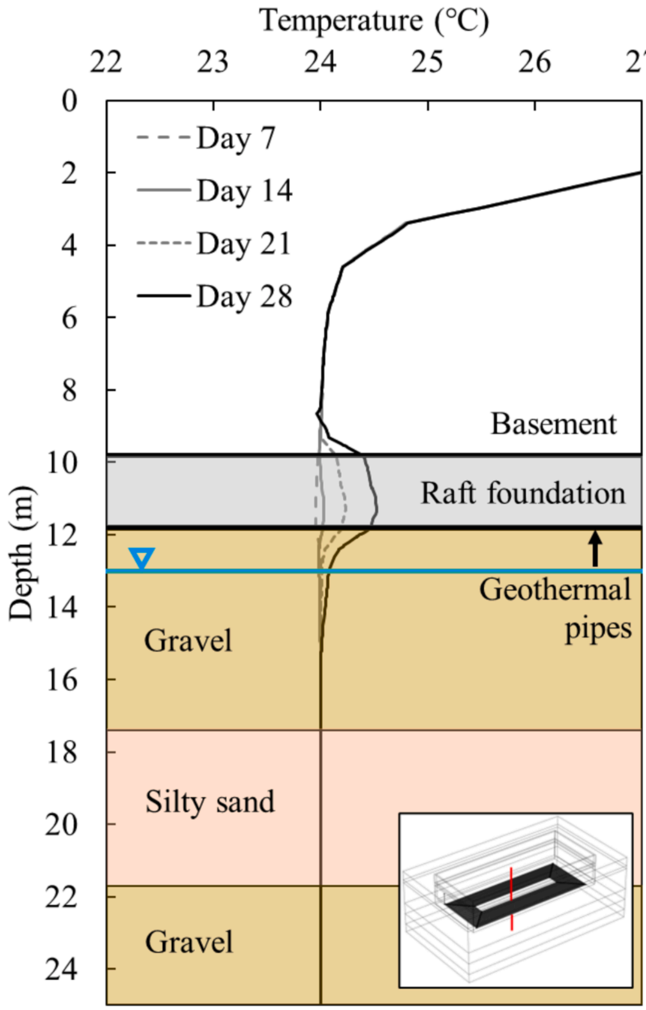

Fig. 8. Soil temperature profiles at the center of the pipe loop.

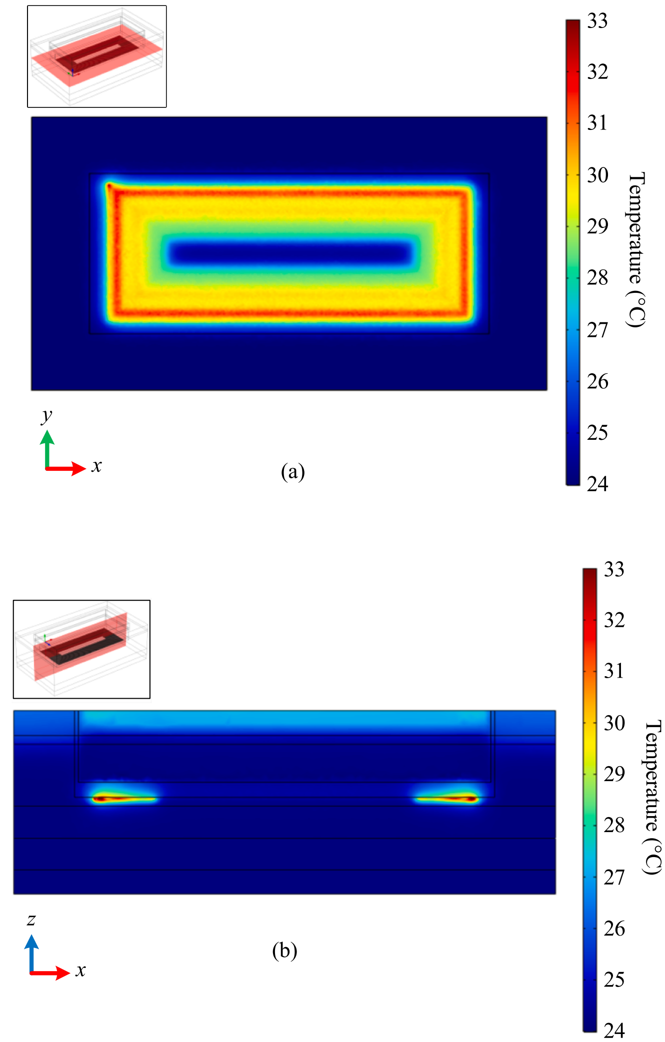

Fig. 9. Soil temperature distribution contours: (a) horizontal cross-section; (b) vertical cross-section.

4.3. Different modeling schemes for the foundation and basement

Accurately modeling the thermal response of an energy foundation is crucial, but incorporating detailed representations of all soil and structural elements can greatly increase computational demands, especially when materials with distinct thermal conductivities are involved (Makasis et al., 2020). Therefore, the analyses reported in this section aimed to reduce the computational time and potential numerical instability due to heat transfer through different materials while also evaluating the effect of the modeling scheme, particularly for components such as the raft foundation and basement, on the accuracy of the thermal response of the energy foundation. This evaluation was intended to determine whether a simplified modeling scheme could produce results comparable to the real condition in the field within a shorter computational time.

The numerical model and geothermal pipe pattern (Fig. 4) were unchanged in all analyses in this section, but the schemes for modeling the foundation structure and basement were varied. Table 3 summarizes the modeling schemes for the foundation structure and basement. In the soil–only modeling scheme, the foundation's and basement's thermal and hydraulic properties were considered the same as those of the gravel soil in layer III, simplifying the transfer of heat between different materials. In the soil–concrete modeling scheme, the foundation structure and basement were each modeled as a concrete block with corresponding thermal and hydraulic properties (Table 2). Finally, in the soil–concrete–air modeling scheme, the raft foundation was modeled as concrete, and the basement was modeled as air. The thermal and hydraulic properties of the concrete and air are listed in Table 2.

Simulations with the soil–concrete modeling scheme took approximately 14 h (using a Core i9-13900F CPU, 64 GB RAM). However, the analysis time significantly increased to 23 h for the soil–concrete–air modeling scheme due to the added complexity of simulating heat transfer between materials with distinct thermal conductivity.

Fig. 11 presents the soil temperature distribution along the longitudinal cross-section at day 28 for each modeling scheme. The soil temperature distributions were similar for the soil–concrete and soil–concrete–air schemes because temperature variation mainly occurred in the concrete raft foundation. Temperatures were higher for the soil-only scheme than the other modeling schemes (by 0.8 °C on average on the top of the geothermal pipe). Fig. 12 compares the soil temperature profile at the center of the pipe loop for the three schemes; the soil–only modeling scheme had the lowest temperature within the raft foundation due to the lower thermal conductivity of the dry soil (λ = 0.6 W/m·K) than that of the concrete (λ = 2.5 W/m·K). The low λ value of the dry soil hindered the dissipation of heat toward the center of the loop. By contrast, similar trends were obtained for the soil–concrete, and soil–concrete–air schemes; temperatures were high within the raft foundation, and the temperature within the basement gradually decreased. Less heat dissipated from the raft foundation to the basement in the soil–concrete–air model than in the soil–concrete model due to the low thermal conductivity value of the air (λ = 0.03 W/m·K).

Fig. 13 shows the outlet fluid temperature at the steady state for the

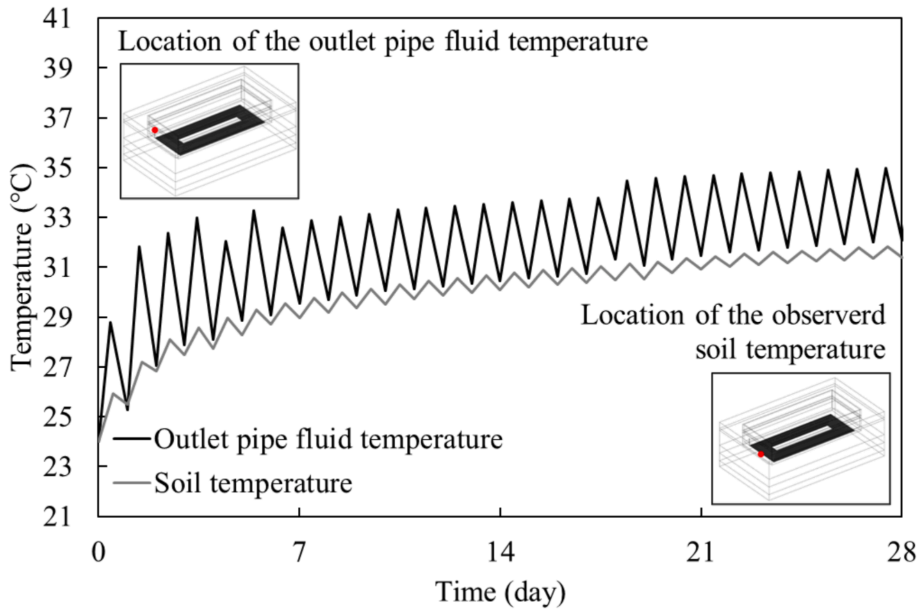

Fig. 10. Variation of geothermal pipe outlet fluid temperature and soil temperature with time.

Table 3
Materials for modeling foundation and basement.

Items	Soil layer	Foundation structure	Basement area
Soil only	Soil	Soil	Soil
Soil-concrete	Soil	Concrete	Concrete
Soil-concrete-air	Soil	Concrete	Air

soil–only, soil–concrete, and soil–concrete–air modeling schemes. Similar to the results shown in Fig. 11, the soil-only model had a higher outlet fluid temperature (by 1 °C; Fig. 13) than did the soil–concrete and soil–concrete–air modeling schemes because the dry soil had lower thermal conductivity than the concrete, resulting in less efficient heat transfer from the pipe fluid to the soil. The trends in the outlet fluid temperature for the soil–concrete and the soil–concrete–air schemes were again similar because the temperature variation mainly occurred within the concrete raft foundation. In summary, the thermal response of the energy raft foundation was discovered to be highly dependent on its thermal properties. The simplified modeling scheme in which the concrete was replaced with soil resulted in an underestimation of the temperature in soil and concrete but an overestimation of the outlet fluid temperature. Therefore, accurate representation of the foundation and basement materials in the model is essential.

5. Parametric study

A series of parametric studies was conducted to evaluate the effects of the geothermal pipe spacing and pattern on the heat exchange efficiency. Table 4 summarizes the pipe spacings and patterns used in the parametric study. The optimal geothermal pipe configuration was determined on the basis of the parametric study results.

The geometry and boundary conditions of the numerical model used in the parametric studies were those of the validated numerical model

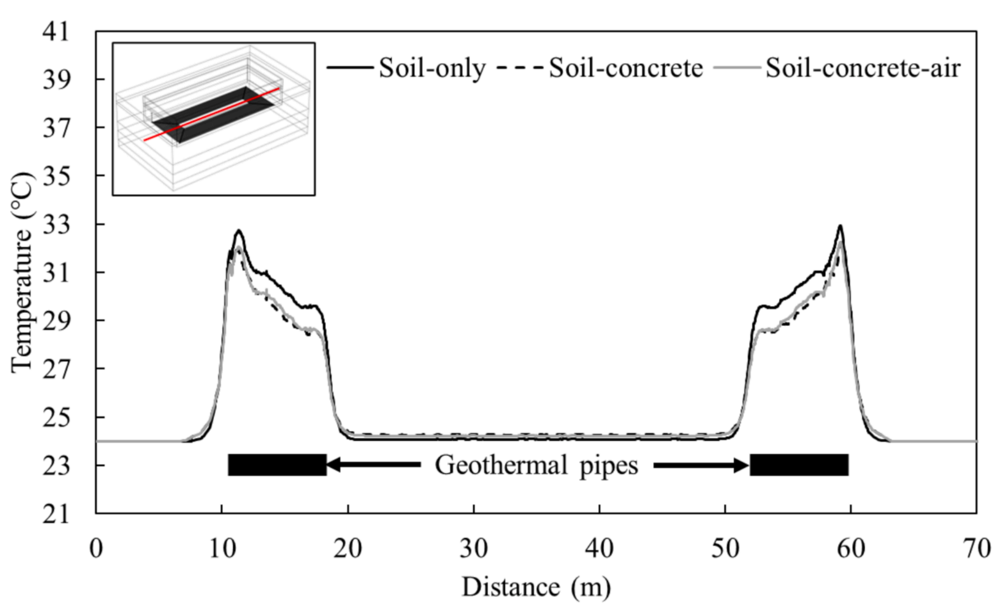

Fig. 11. Comparison of soil temperature distributions along the longitudinal cross-section for different modeling schemes for the foundation and basement.

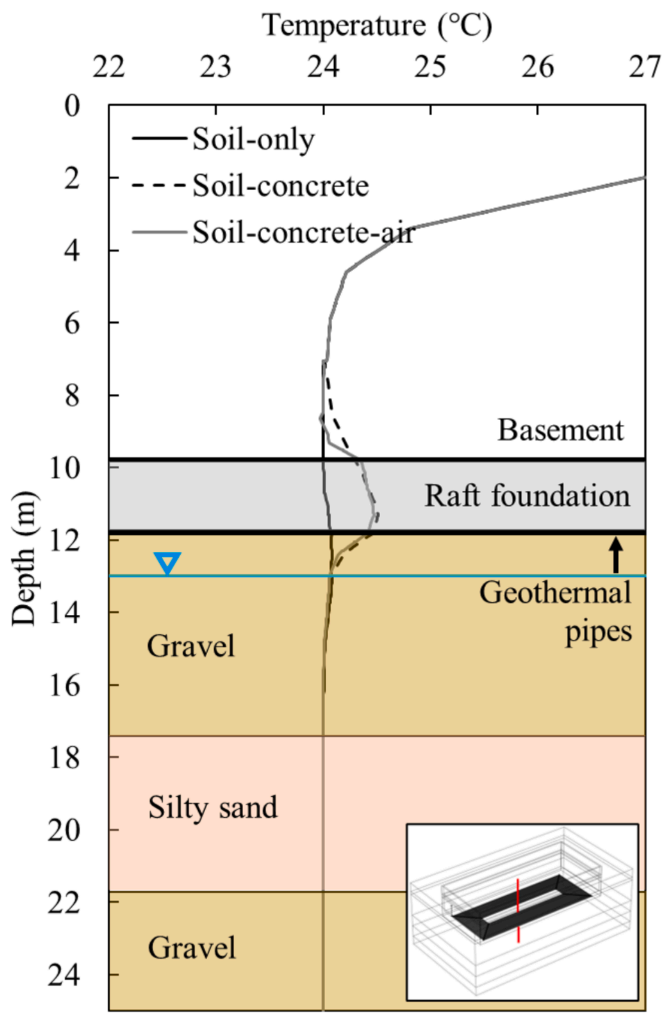

Fig. 12. Comparison of soil temperature profiles for different modeling schemes for the foundation and basement.

(Fig. 4). However, for simplification, the numerical model only included one type of soil (gravel), which was given the thermal and hydraulic properties corresponding to layer III (Table 2) and had a constant $T_{initial}$ = 24 °C. The geothermal pipe spacing and pipe pattern were varied, as listed in Table 4, to investigate their influences on the pipe outlet fluid and soil temperature. The pumping power of the GSHP system in the parametric study was assumed to be sufficient to circulate the fluid effectively.

5.1. Influence of geothermal pipe spacing

This section investigated six pipe spacings: S = 0.1, 0.5, 1, 2, 3, and 4 m. For each pipe spacing, the pipe length was different; larger spacing required shorter pipes to maintain a coverage area of 49.3 m × 19.8 m (Fig. 4b).

Fig. 14 presents the average soil and geothermal outlet fluid temperature for each pipe spacing. The average soil temperature was calculated by averaging the soil temperature across the width of the geothermal pipe loop at the steady state. The soil temperature consistently decreased as the pipe spacing increased because pipe loops with larger spacings had a shorter total length available for heat exchange. Therefore, less heat was transferred from the pipe to the soil, resulting in a lower soil temperature for a larger spacing.

The spacing that minimized the outlet fluid temperature (i.e., maximized the temperature difference between the outlet and inlet) was identified. The pipe outlet fluid temperature was high at 35.6 °C for S = 0.1 m and 37.1 °C for S = 4 m. Increasing the pipe spacing from S = 0.1 m to S = 0.5 m, which corresponded to a reduction in pipe length L to 1805 m, decreased the outlet fluid and soil temperatures by 2.3 and 0.8 °C, respectively. Further increases in the spacing, accompanied by corresponding reductions in L, increased the outlet fluid temperature and decreased the average soil temperature.

The high outlet fluid temperature at S = 0.1 m was attributable to heat accumulation in the soil and the influence of the high-temperature adjacent pipe. Heat accumulation caused a decrease in the temperature

Table 4
Parametric study program.

Variables	Items and values
Pipe spacings (m) (⊔)	0.1, 0.5, 1, 2, 3, 4
Geothermal pipe patterns	Snake, Meander, Loop, Swirl for S = 0.1 and 1 m

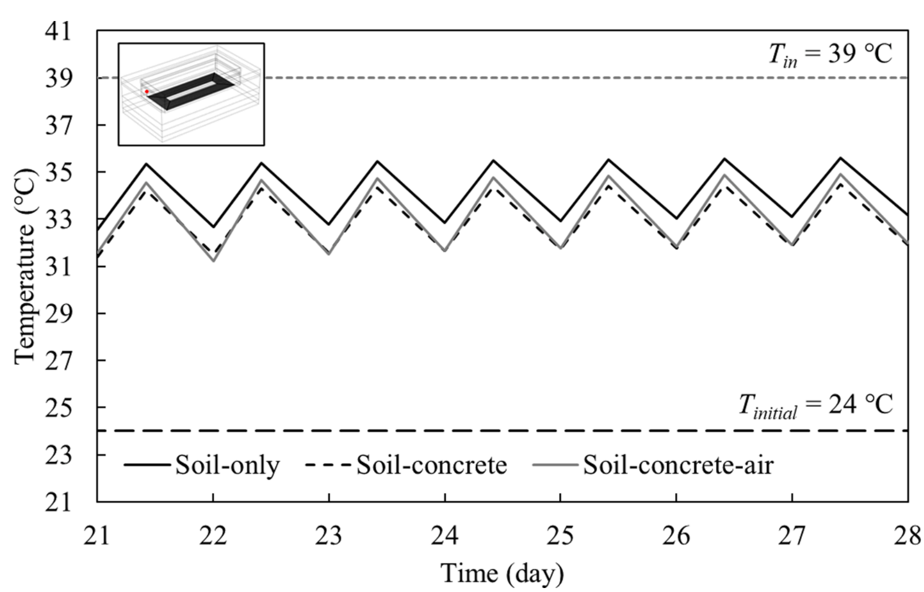

Fig. 13. Comparison of geothermal pipe outlet fluid temperatures for different modeling schemes for the foundation and basement.

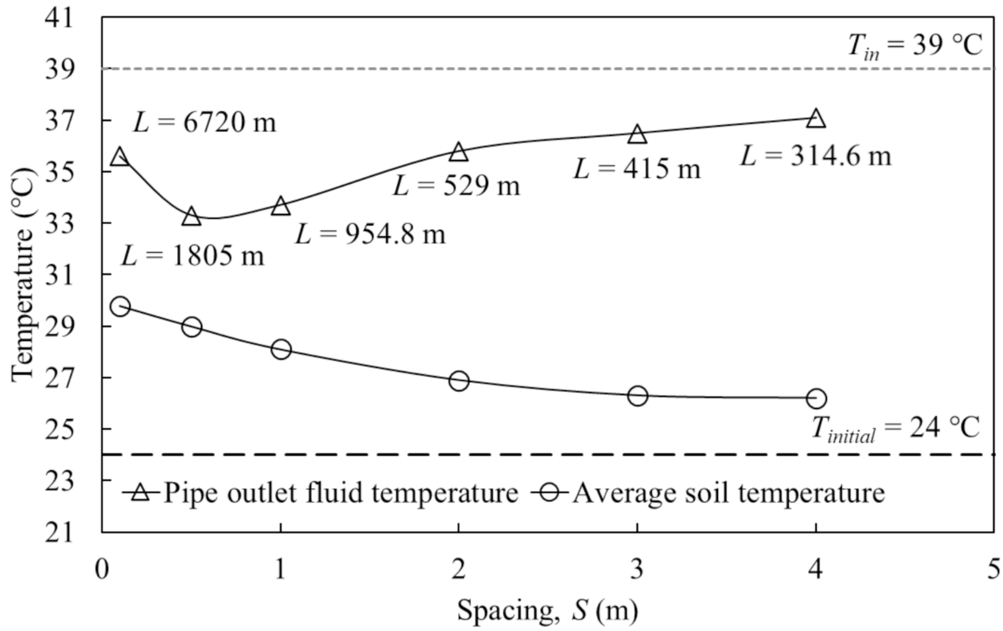

Fig. 14. Variation in average soil temperature and geothermal pipe outlet fluid temperature for different geothermal pipe spacings.

gradient between the geothermal pipe and the soil, decreasing heat exchange efficiency. Fig. 15 presents the thermal interaction between adjacent pipes. For $S = 0.1$ m (Fig. 15a), the fluid temperature increased gradually from 35.5 to 35.7 °C as the fluid approached the outlet. This phenomenon indicated thermal interaction between adjacent pipes in the inlet and outlet directions but was not observed in configurations with larger S (Fig. 15b and 15c). When $S > 0.5$ m, the outlet fluid temperature increased as the pipe spacing was increased. This trend was attributable to the larger spacing decreasing the total length available for heat exchange, resulting in high outlet fluid temperature.

The results presented in Fig. 14 revealed that the geothermal pipe spacing of $S = 0.5$ m resulted in the lowest outlet fluid temperature at 33.3 °C. However, a spacing of $S = 1$ m was identified as the optimal value in this study; although the outlet fluid temperature was 0.4 °C higher for $S = 1$ m than for $S = 0.5$ m, $S = 1$ m resulted in 47 % lower total pipe length. This approach involved finding the balance between the heat exchange efficiency and the use of pipe material for the optimal design of an energy raft foundation.

5.2. Influence of geothermal pipe pattern

Four pipe patterns (i.e., snake, meander, loop, and swirl; Table 4) were considered to investigate the influence of pattern on the pipe outlet fluid and soil temperature. Fig. 16 displays the pipe patterns in the numerical model; red and blue lines indicate the first and second halves of the geothermal pipe, respectively. For the snake and swirl patterns (Fig. 16a and 16d), the first and second halves of the pipe were separate, whereas, for the meander and loop patterns (Fig. 16b and 16c), the first and second halves of the pipe were alternately arranged. Two pipe spacings were considered for each pattern (i.e., $S = 0.1$ and 1 m); the

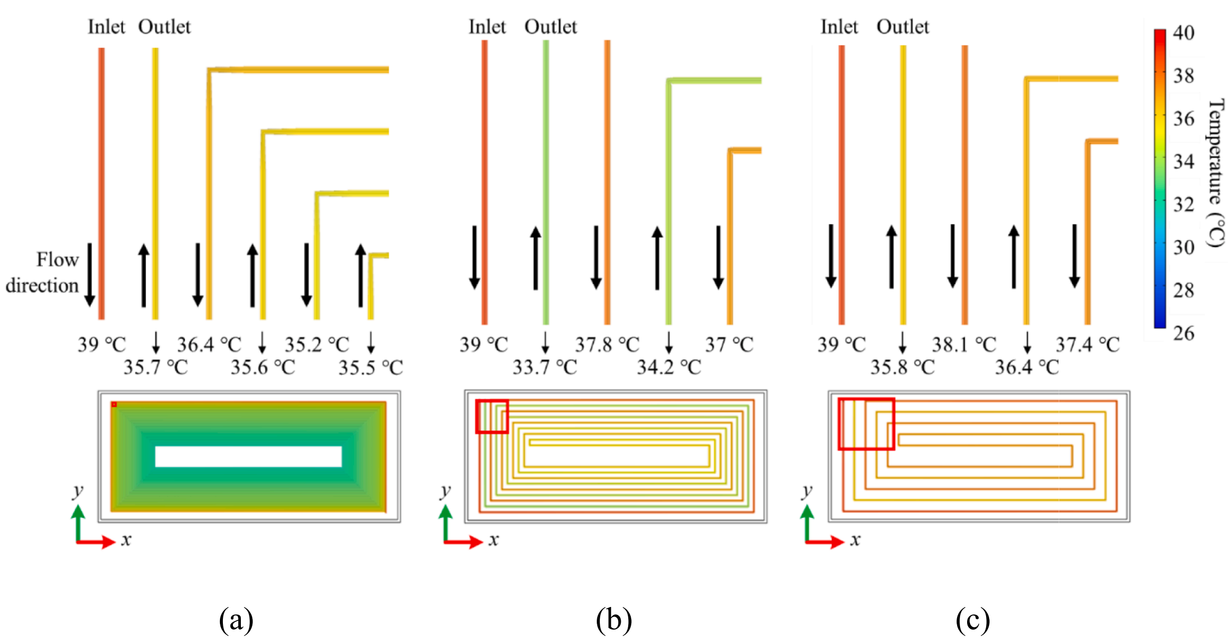

Fig. 15. Geothermal pipe temperatures for different pipe spacings: (a) 0.1 m, (b) 1 m, and (c) 2 m.

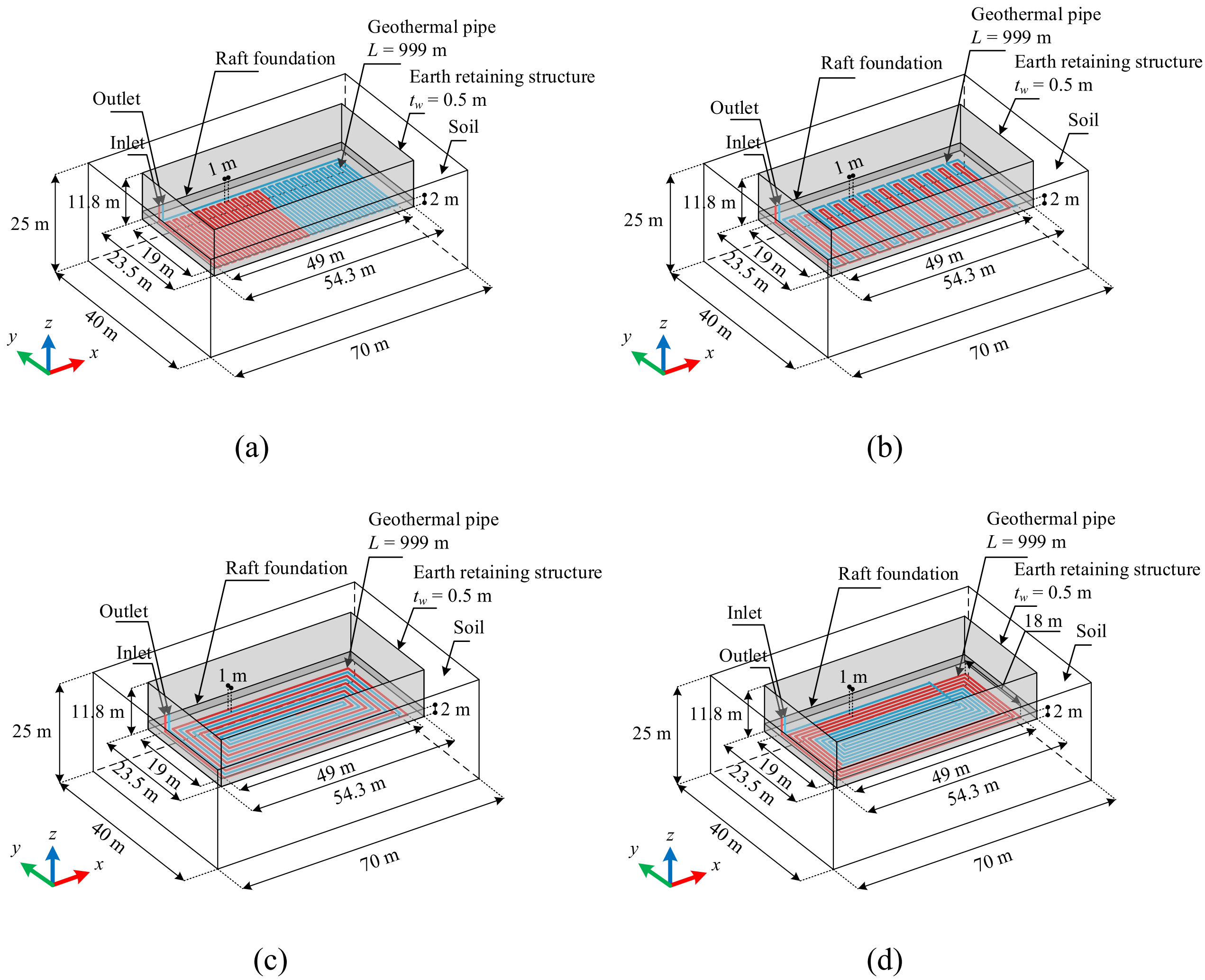

Fig. 16. Geothermal pipe patterns: (a) snake; (b) meander; (c) loop; (d) swirl for $S = 1$ m (Note that the red and blue lines indicate the first and second halves of the geothermal pipe, respectively). (For interpretation of the references to colour in this figure legend, the reader is referred to the web version of this article.)

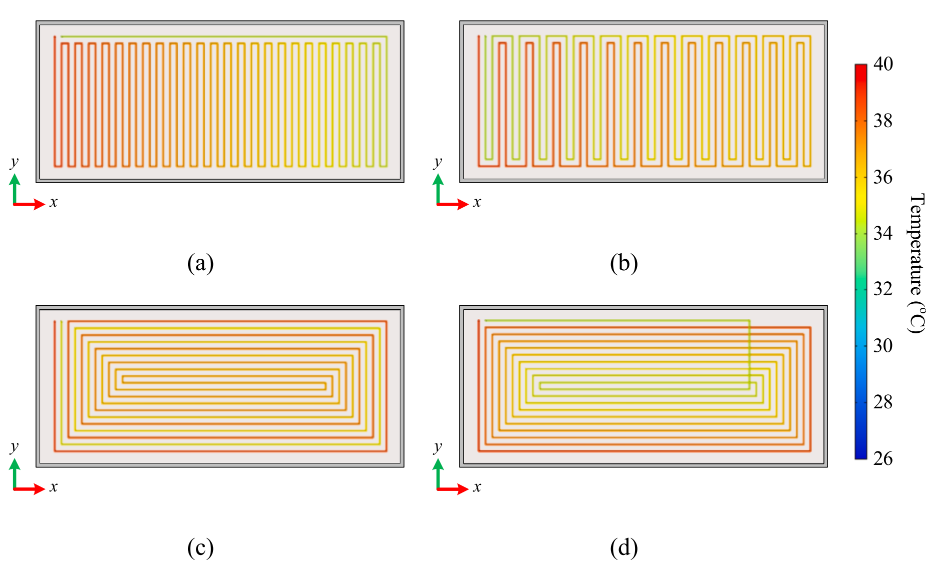

Fig. 17. Geothermal pipe temperature distribution contour for different patterns: (a) snake; (b) meander; (c) loop; (d) swirl with $S = 1$ m.

corresponding total lengths were $L = 9348$ and 999 m, respectively. All patterns covered an area of 49 m × 19 m at a depth of 12 m.

Fig. 17 displays the geothermal pipe temperature distribution contours for different patterns with $S = 1$ m. In the snake pattern (Fig. 17a), the high inlet fluid temperature, indicated by red, gradually decreased as the fluid flowed toward the left boundary of the pattern and continued flowing toward the right boundary and the pipe outlet; it reached the outlet at a temperature of 34.3 °C. Similarly, in the meander pattern (Fig. 17b), the temperature was high near the inlet and steadily decreased as the fluid flowed along the pipe toward the outlet, ultimately being 34.3 °C. In the loop pattern (Fig. 17c), the temperature decreased as the fluid flowed counterclockwise from the inlet toward the center of the pattern. As it continued by flowing clockwise, the fluid reached the outlet at 34.9 °C at the steady state. Finally, for the swirl pattern (Fig. 17d), the temperature gradually decreased as the fluid flowed counterclockwise from the inlet toward the center of the pattern; the outlet fluid temperature was 34.4 °C.

Fig. 18 displays the outlet fluid temperature for each geothermal pipe pattern given pipe spacings of $S = 0.1$ and 1 m. The pipe spacing–pattern combination strongly influenced the heat exchange efficiency. At $S = 0.1$ m, the outlet fluid temperatures for the snake, meander, loop, and swirl patterns were 32.5, 34.9, 35.6, and 32.3 °C, respectively. The meander and loop patterns had higher outlet fluid temperatures (i.e., lower heat exchange efficiency) than the snake and swirl patterns. The high outlet fluid temperature observed for the meander and loop patterns was attributable to the thermal interaction between the first and second halves of the pipe at the close spacing of $S =$ 0.1 m. This thermal influence between the first and second halves of the pipes resulted in a higher temperature. Conversely, heat exchange was more efficient for the snake and swirl patterns at the smaller spacing because the interactions between the high-temperature first half and low-temperature second half were negligible.

For the pipe spacing of $S = 1$ m, the outlet fluid temperature was similar for all pipe patterns, being in the range 34.3–34.9 °C; the loop pattern resulted in the highest value. This result suggested that the pipe pattern had a minimal influence on the heat exchange efficiency when the pipe spacing was sufficiently large because adjacent pipes did not influence each other. In summary, for the snake and swirl patterns, the pipe outlet fluid temperature was lowest for a pipe spacing of $S = 0.1$ m due to the long pipes available for heat exchange. For the meander and loop patterns, the pipe outlet fluid temperature at $S = 0.1$ m was higher than that at $S = 1.0$ m due to the influence of adjacent pipes.

6. Conclusions

This paper presents a numerical investigation into the thermal response of an energy raft foundation in Taipei. A three-dimensional finite element model was developed using COMSOL Multiphysics and validated against field measurements. A series of parametric studies was then conducted to evaluate the effects of geothermal pipe spacing and patterns on heat exchange efficiency. On the basis of the findings of this study, several key conclusions can be drawn:

- The numerical model of the energy raft foundation successfully captured the actual thermal behavior of the geothermal system.
- The results from the case study indicated that the soil and pipe outlet fluid temperatures increased over time; a steady state condition was reached after approximately 3 weeks of operation. The maximum and minimum temperature differences between the inlet and outlet fluid temperatures were 7 and 4 °C, occurring at the daily operation's beginning and end, respectively.
- Analyses of the temperature distributions revealed that the horizontal range of influence of the geothermal pipe on the soil temperature was small at approximately 1.6 times the width of the pipe loop, suggesting that the geothermal pipe would have little influence on the temperature of the soil in an adjacent building's foundation.
- Through analyses of the influences of geothermal pipe spacing on the pipe outlet fluid and soil temperature, the optimal spacing of $S = 1$ m was identified; this spacing minimized the outlet fluid temperature (or maximized the temperature difference between the outlet and inlet). For a pipe spacing of $S = 0.1$ m, the outlet fluid temperature was high because of heat accumulation in the soil (reducing the temperature gradient between the geothermal pipe and the soil and thus decreasing the heat exchange efficiency). The outlet fluid temperature also increased due to heat transfer from adjacent pipes in this small-pipe-spacing scenario. At pipe spacings of $S > 0.5$ m, the outlet fluid temperature increased with increasing pipe spacing because the total length of pipe available for heat exchange was smaller.
- Analyses of the influence of the geothermal pipe pattern on the heat exchange efficiency revealed that the pipe outlet fluid temperature depended strongly on the pipe spacing. For the snake and swirl patterns, the pipe outlet fluid temperature was lowest for a pipe spacing of $S = 0.1$ m due to the large pipe length available for heat exchange. For the meander and loop patterns, the pipe outlet fluid temperature at $S = 0.1$ m was higher than that at $S = 1.0$ m due to the influence of adjacent pipes.

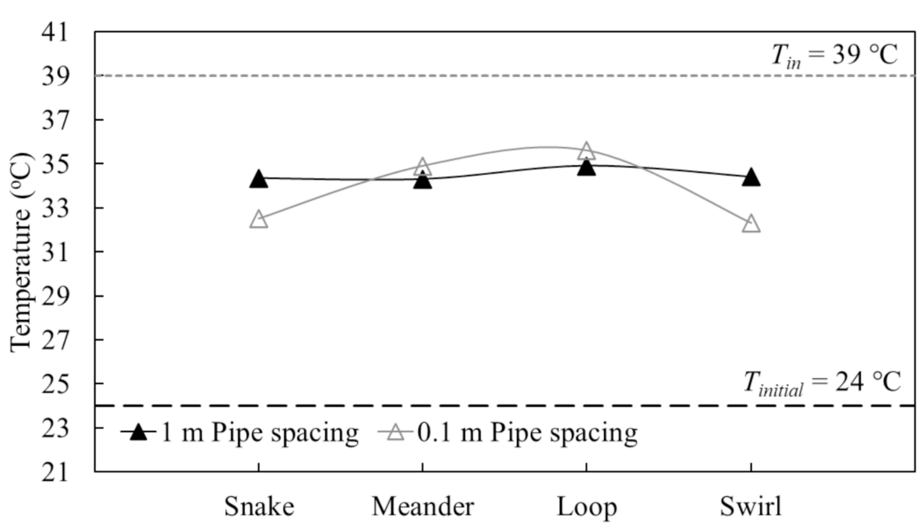

Fig. 18. Comparison of the geothermal pipe outlet fluid temperature for various geothermal pipe patterns.

This study was focused on the thermal response of an energy raft foundation. The long-term thermal response of energy raft foundations should be investigated in future research to confirm the range of influence on the soil temperature for a geothermal pipe. The mechanical behavior of an energy raft foundation is crucial to the stability and serviceability of the structure. Further investigation of the mechanical behavior of an energy raft foundation, such as thermal-induced stress in the concrete slab and the reaction force from the thermal expansion acting on the soil, should be conducted in future research.

CRediT authorship contribution statement

Ignatius Tommy Pratama: Writing – original draft, Visualization, Software, Formal analysis, Data curation. **Josiane Jello:** Writing – original draft, Software, Formal analysis, Data curation. **Xin-Bai Mao:** Software, Formal analysis, Data curation. **Kuo-Hsin Yang:** Writing – original draft, Validation, Supervision, Resources, Project administration, Methodology, Investigation, Funding acquisition, Conceptualization. **Jui-Pin Tsai:** Supervision, Resources. **Tugce Baser:** Writing – original draft, Validation, Supervision, Resources, Project administration, Investigation, Funding acquisition, Conceptualization. **Chihping Kuo:** Supervision, Resources.

Declaration of competing interest

The authors declare that they have no known competing financial interests or personal relationships that could have appeared to influence the work reported in this paper.

Acknowledgment

The case study presented in this paper was designed and built by the Fabulous Group. The authors extend sincere gratitude to Fabulous Group for providing the design and construction details. This research was supported by the National Taiwan University (NTU) and University of Illinois (U of I) Joint Research and Innovation Seed Grants.

Data availability

Data will be made available on request.

References

Alnefaie, K.A., Abu-Hamdeh, N.H., 2020. Specific heat and volumetric heat capacity of some Saudian soils as affected by moisture and density. Int. J. Mater. 7, 42–46. https://doi.org/10.46300/91018.2020.7.8.

Amirdehi, H.A., Shooshpasha, I., 2022. Evaluation of coupled interaction effects caused by the long-term performance of energy piles in a piled raft foundation. Geotech. Geol. Eng. 40 (10), 5153–5180. https://doi.org/10.1007/s10706-022-02209-3.

Angelotti, A., Sterpi, D., 2020. On the performance of energy walls by monitoring assessment and numerical modelling: a case in Italy. Environ. Geotechnics 7 (4), 266–273. https://doi.org/10.1680/jenge.18.00037.

Barla, M., Di Donna, A., Insana, A., 2019. A novel real-scale experimental prototype of energy tunnel. Tunn. Undergr. Space Technol. 87, 1–14. https://doi.org/10.1016/j.tust.2019.01.024.

Baser, T., Dong, Y., Moradi, A.M., Lu, N., Smits, K., Ge, S., Tartakovsky, D., McCartney, J. S., 2018. Role of nonequilibrium water vapor diffusion in thermal energy storage systems in the vadose zone. J. Geotech. Geoenviron. Eng. 144 (7), 04018038. https://doi.org/10.1061/(ASCE)GT.1943-5606.0001910.

Behbehani, F., McCartney, J.S., 2022. Energy pile groups for thermal energy storage in unsaturated soils. Appl. Therm. Eng. 215, 119028. https://doi.org/10.1016/j.applthermaleng.2022.119028.

Bejan, A., 2013. Convection heat transfer. John Wiley & Sons Inc., Hoboken, NJ, USA.

Bourne-Webb, P.J., Freitas, T.B., da Costa Gonçalves, R.A., 2016. Thermal and mechanical aspects of the response of embedded retaining walls used as shallow geothermal heat exchangers. Energy Build. 125, 130–141. https://doi.org/10.1016/j.enbuild.2016.04.075.

Brandl, H., 2006. Energy foundations and other thermo-active ground structures. Géotechnique 56 (2), 81–122. https://doi.org/10.1680/geot.2006.56.2.81.

Cao, Q., Gong, S., Li, P., Wan, H., Cheng, D., 2018. Correlation analysis of thermal physical indexes in subway engineering. IOP Conf. Ser.: Mater. Sci. Eng. 394, 032051. https://doi.org/10.1088/1757-899X/394/3/032051.

Casagrande, B., Saboya Jr, F., McCartney, J.S., Tibana, S., 2022. Investigation of a field-scale energy micropile in stratified soil under cyclic temperature changes. Geomech. Energy Environ. 29, 100263. https://doi.org/10.1016/j.gete.2021.100263.

Caulk, R., Ghazanfari, E., McCartney, J.S., 2016. Parameterization of a calibrated geothermal energy pile model. Geomech. Energy Environ. 5, 1–15. https://doi.org/10.1016/j.gete.2015.11.001.

Coccia, C.J., McCartney, J.S., 2016. Impact of long-term temperature cycling on the thermo-hydro-mechanical behavior of unsaturated soils surrounding an energy pile. In: Geo-Chicago 2016, pp. 42-51. doi: 10.1061/9780784480137.005.

COMSOL Multiphysics, 2023a. Pipe flow module user's guide 6.2. Burlington, MA, USA: COMSOL Inc.

COMSOL Multiphysics, 2023b. Heat transfer module user's guide 6.2. Burlington, MA, USA: COMSOL Inc.

COMSOL Multiphysics, 2023c. CFD module user's guide 6.2. Burlington, MA, USA: COMSOL Inc.

Cunha, R.P., Bourne-Webb, P.J., 2022. A critical review on the current knowledge of geothermal energy piles to sustainably climatize buildings. Renew. Sustain. Energy Rev. 158, 112072. https://doi.org/10.1016/j.enbuild.2016.04.075.

Faizal, M., Bouazza, A., McCartney, J.S., 2021. Thermohydraulic responses of unsaturated sand around a model energy pile. J. Geotech. Geoenviron. Eng. 147 (10), 04021105. https://doi.org/10.1061/(ASCE)GT.1943-5606.0002640.

Faizal, M., Bouazza, A., McCartney, J.S., 2022. Thermal resistance analysis of an energy pile and adjacent soil using radial temperature gradients. Renew. Energy 190, 1066–1077. https://doi.org/10.1016/j.renene.2022.04.002.

Di Donna, A., Loveridge, F., Piemontese, M., Barla, M., 2021. The role of ground conditions on the heat exchange potential of energy walls. Geomech. Energy Environ. 25, 100199. https://doi.org/10.1016/j.gete.2020.100199.

Faizal, M., Bouazza, A., Haberfield, C., McCartney, J.S., 2018. Axial and radial thermal responses of a field-scale energy pile under monotonic and cyclic temperature changes. J. Geotech. Geoenviron. Eng. 144 (10), 04018072. https://doi.org/10.1061/(ASCE)GT.1943-5606.0001952.

Faizal, M., Bouazza, A., McCartney, J.S., Haberfield, C., 2019. Axial and radial thermal responses of energy pile under six storey residential building. Can. Geotech. J. 56 (7), 1019–1033. https://doi.org/10.1139/cgj-2018-0246.

Faizal, M., Moradshahi, A., Bouazza, A., McCartney, J.S., 2020. Soil thermal responses around a field-scale energy pile.

Fang, J., Kong, G., Meng, Y., Wang, L., Yang, Q., 2020. Thermomechanical behavior of energy piles and interactions within energy pile–raft foundations. J. Geotech. Geoenviron. Eng. 146 (9), 04020079. https://doi.org/10.1061/(ASCE)GT.1943-5606.0002333.

Fang, W.-T., Chien, C.-P., 2004. Soil column experiment in determining thermal conductivity for fully saturated soils. J. Chinese Agric. Eng. 50 (1), 63–71.

Ghasemi-Fare, O., Basu, P., 2013. A practical heat transfer model for geothermal piles. Energ. Buildings 66, 470–479. https://doi.org/10.1016/j.ijheatmasstransfer.2019.119020.

Insana, A., Barla, M., 2020. Experimental and numerical investigations on the energy performance of a thermo-active tunnel. Renew. Energy 152, 781–792. https://doi.org/10.1016/j.renene.2020.01.086.

Jello, J., Baser, T., 2023. Utilization of existing hydrocarbon wells for geothermal system development: a review. Appl. Energy 348, 121456. https://doi.org/10.1016/j.apenergy.2023.121456.

Khan, M.A., Wang, J.X., 2014. Study on energy foundation design in South Louisiana. In Geo-Congress 2014: Geo-characterization and Modeling for Sustainability, pp. 3799-3806.

Khosravi, A., Moradshahi, A., McCartney, J.S., Kabiri, M., 2016. Numerical analysis of energy piles under different boundary conditions and thermal loading cycles. doi: 10.1051/e3sconf/20160905005.

Laloui, L., Loria, A.F.R., 2019. Analysis and design of energy geostructures: theoretical essentials and practical application. Academic Press.

Lee, S., Park, S., Kang, M., Choi, H., 2018. Field experiments to evaluate thermal performance of energy slabs with different installation conditions. Appl. Sci. 8 (11), 2214. https://doi.org/10.3390/app8112214.

Lee, S., Park, S., Won, J., Choi, H., 2021. Influential factors on thermal performance of energy slabs equipped with an insulation layer. Renew. Energy 174, 823–834. https://doi.org/10.1016/j.renene.2021.04.090.

Liu, Y.-H., 1974. A study of the microclimate of Taipei basin. Atmospheric Science 1 (1), 1–20.

Lund, J.W., Toth, A.N., 2021. Direct utilization of geothermal energy 2020 worldwide review. Geothermics 90, 101915. https://doi.org/10.1016/j.geothermics.2020.101915.

Makasis, N., Narsilio, G.A., Bidarmaghz, A., Johnston, I.W., Zhong, Y., 2020. The importance of boundary conditions on the modelling of energy retaining walls. Comput. Geotech. 120, 103399. https://doi.org/10.1016/j.compgeo.2019.103399.

McCartney, J., Coccia, C., Alsherif, N., Stewart, M., Baser, T., Traore, T., Goode, J., 2014. Unsaturated soil mechanics in geothermal energy applications. doi: 10.1201/b17034-119.

Mehrizi, A.A., Porkhial, S., Bezyan, B., Lotfizadeh, H., 2016. Energy pile foundation simulation for different configurations of ground source heat exchanger. Int. Commun. Heat Mass Transfer 70, 105–114. https://doi.org/10.1016/j.icheatmasstransfer.2015.12.001.

Mendrinos, D., Katsantonis, S., Karytsas, C., 2017. Review of alternative pipe materials for exploiting shallow geothermal energy. Innovations in Corrosion and Materials Science (formerly Recent Patents on Corrosion Science) 7 (1), 13–29. https://doi.org/10.2174/2352094907666170327163227.

Moon, C.E., Choi, J.M., 2015. Heating performance characteristics of the ground source heat pump system with energy-piles and energy-slabs. Energy 81, 27–32. https://doi.org/10.1016/j.energy.2014.10.063.

Moradshahi, A., Faizal, M., Bouazza, A., McCartney, J.S., 2022. Thermomechanical responses of thermally interacting field-scale energy piles. Int. J. Geomech. 22 (11), 04022212. https://doi.org/10.1061/(ASCE)GM.1943-5622.0002523.

Reiter, M.B., Jello, J., Baser, T., 2023. Thermo-hydro-mechanical behavior of energy foundations in saturated glacial tills. Geothermics 108, 102614. https://doi.org/10.1016/j.geothermics.2022.102614.

Reiter, M.B., Kurtz, L., Attala, M.M., Baser, T., 2020. Changes in shaft resistance and pore water pressures during heating of an energy foundation. In: E3S Web of Conferences, vol. 205. EDP Sciences, p. 05022, doi: 10.1051/e3sconf/202020505021.

Sani, A.K., Singh, R.M., Amis, T., Cavarretta, I., 2019. A review on the performance of geothermal energy pile foundation, its design process and applications. Renew. Sustain. Energy Rev. 106, 54–78. https://doi.org/10.1016/j.rser.2019.02.008.

Santa, G.D., Peron, F., Galgaro, A., Cultrera, M., Bertermann, D., Mueller, J., Bernardi, A., 2017. Laboratory measurements of gravel thermal conductivity: an update methodological approach. Energy Procedia 125, 671–677. https://doi.org/10.1016/j.egypro.2017.08.287.

Singh, R.M., Bouazza, A., Wang, B., Haberfield, C.H., Baycan, S., Carden, Y., 2015. Thermal and thermo-mechanical response of a geothermal energy pile. In World Geothermal Congress 7.

ten Bosch, S., Ravera, E., Laloui, L., 2024. Performance of energy piles foundation in hot-dominated climate: a case study in Dubai. Renew. Energy 220, 119632. https://doi.org/10.1016/j.renene.2023.119632.

You, S., Cheng, X., Guo, H., Yao, Z., 2016. Experimental study on structural response of CFG energy piles. Appl. Therm. Eng. 96, 640–651. https://doi.org/10.1016/j.applthermaleng.2015.11.127.

Zhong, Y., Bidarmaghz, A., Narsilio, G.A., Makasis, N., 2023. Thermo-hydraulic analysis in geothermal energy walls. Tunn. Undergr. Space Technol. 132, 104862. https://doi.org/10.1016/j.tust.2022.104862.